ACS OMEGA

Open Access

http://pubs.acs.org/journal/acsodf

Article

Low-Temperature Thermal Transport Characteristics in Epitaxial Bilayer Graphene Microbridges

Feiming Li, Wei Miao,* Cui Yu, Zezhao He, Qingcheng Wang, Jiaqiang Zhong, Feng Wu, Zheng Wang, Kangmin Zhou, Yuan Ren, Wen Zhang, Jing Li, Shengcai Shi, Qingbin Liu, and Zhihong Feng*

Cite This: *ACS Omega* 2024, 9, 23053−23059

Read Online

ACCESS | Metrics & More | Article Recommendations

ABSTRACT: In this paper, we present a study of the thermal transport of epitaxial bilayer graphene microbridges. The thermal conductance of three graphene microbridges with different lengths was measured at different temperatures using Johnson noise thermometry. We find that with the decrease of the temperature, the thermal transport in the graphene microbridges switches from electron−phonon coupling to electron diffusion, and the switching temperature is dependent on the length of the microbridge, which is in good agreement with the simulation based on a distributed hot-spot model. Moreover, the electron−phonon thermal conductance has a temperature power law of T^3 as predicted for pristine graphene and the electron−phonon coupling coefficient σ_{ep} is found to be approximately 0.18 W/(m^2 K^4), corresponding to a deformation potential D of 55 eV. In addition, the electron diffusion in the graphene microbridges adheres to the Wiedemann−Franz law, requiring no corrections to the Lorentz number.

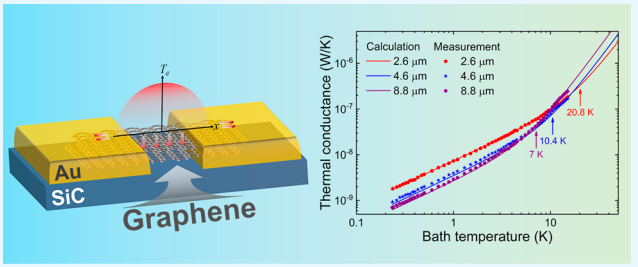

INTRODUCTION

The remarkable properties of graphene, characterized by its small electronic heat capacity,[1] weak electron−phonon interaction,[2] and high intrinsic mobility,[3] have sparked much interest in utilizing it for ultrafast and ultrasensitive detectors. The experimental realization of the first graphene-based hot electron bolometer (HEB) by Yan et al. in 2012[4] has catalyzed extensive efforts to develop highly sensitive graphene-based HEBs. These efforts include the novel approaches such as patterning quantum dots[5] or introducing defects to induce strong localization[6] in graphene. Beyond HEBs, graphene has also been explored in the realms of field effect transistors (FETs)[7−9] and Josephson detectors,[10−12] diversifying its applications in electronic devices. However, for the development of highly sensitive graphene-based detectors, a profound understanding of thermal transport in graphene is paramount. Thermal transport not only determines the ultimate sensitivity of HEBs and Josephson detectors but also imposes the fundamental limit on the mobility of charge carriers in FETs. At present, there are several methods to study thermal transport in graphene, namely, to access the electron temperature and determine the thermal conductance, with noise thermometry being a notable technique.[13−15] Noise thermometry directly probes the electron temperature by measuring the microwave frequency Johnson noise emitted by electrons in graphene. Additionally, electron temperature can be deduced by observing the behavior of Josephson junctions[16] or measuring the quantum Hall effect in graphene[17] within certain temperature regimes. Superconducting tunnel spectroscopy has also contributed to the understanding of nonequilibrium energy distribution and cooling mechanisms in graphene.[18] In this paper, we present the study of thermal transport in quasi-freestanding epitaxial bilayer graphene.[19,20] The thermal conductance of three graphene microbridges with different lengths is measured at different temperatures using Johnson noise thermometry. The measured results are then compared with the simulation based on a distributed hot spot model,[18,21] providing insights into the thermal behavior of the graphene microbridges. In addition, the influence of an external magnetic field on the thermal conductance of the graphene microbridge is also discussed.

The devices used in our measurements were made from quasi-freestanding epitaxial bilayer graphene. This graphene was produced by annealing as-prepared monolayer graphene in molecular hydrogen, a process designed to decouple the graphene layer from the silicon carbide (SiC) substrate.[19,20] As a result, the bilayer graphene exhibits p-type doping, with a carrier mobility μ of ∼4070 cm^2/(V s) and a charge carrier density n of ∼1.2 × 10^{13} cm^{-2}. It yields an electrical mean free

Received: March 20, 2024
Revised: April 25, 2024
Accepted: May 7, 2024
Published: May 14, 2024

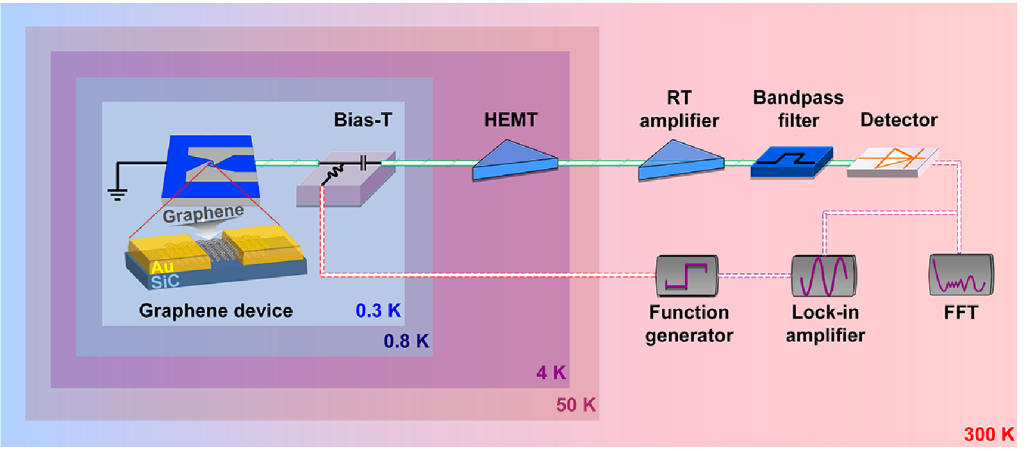

Figure 1. Schematic of the measurement setup based on Johnson noise thermometry. The function generator administers modulated square wave voltage excitation to the graphene device. The Johnson noise signal from the graphene device is amplified by both a cryogenic low-noise amplifier and a room-temperature amplifier. Following filtration through a bandpass filter to specify the readout bandwidth, the Johnson noise signal proceeds through a square-law detector for readout. The FFT analyzer determines the noise power spectral density, while the lock-in amplifier captures the response value. On the left is a structure diagram of the graphene device, featuring a graphene microbridge connected to Au contact electrodes and then linked to a log spiral antenna.

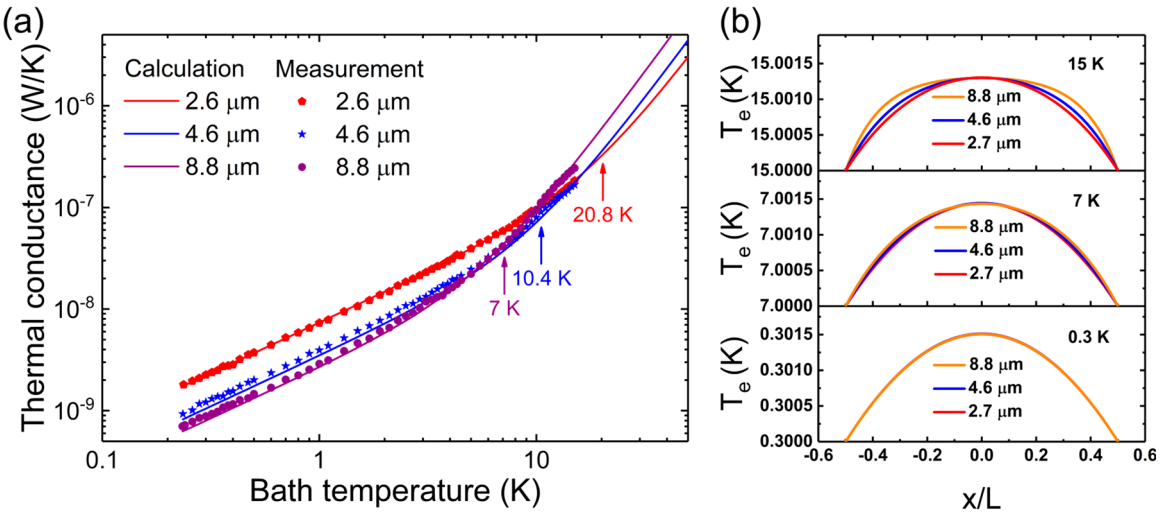

Figure 2. (a) Measured thermal conductance of three graphene devices with different microbridge lengths at different temperatures, together with the simulated results based on a distributed hot spot model. (b) The calculated electron temperature distributions of three graphene devices at bath temperatures of 0.3, 7, and 15 K, respectively.

path l_e of ∼166 nm in terms of $l_e = h\mu(n/\pi)^{0.5}/2e$,[22] where h is the Planck constant and e is the elementary charge. Utilizing this bilayer graphene, we fabricated three graphene devices with different microbridge lengths through the application of standard optical lithography and lift-off processes. The structure diagram of a graphene device is depicted on the left side of Figure 1, featuring a graphene microbridge connected to gold (Au) contact electrodes and, subsequently, to a log spiral antenna, designed for terahertz radiation coupling. In our case, three graphene devices were produced, with microbridge lengths of 2.7 μm, 4.6 μm, and 8.8 μm, while their microbridge widths remain consistently at approximately 9.6 μm. The corresponding direct current (dc) resistances for these graphene devices are 40.1, 85.1, and 112.4 Ω at room temperature.

Figure 1 illustrates the schematic diagram of the measurement setup for the graphene devices based on Johnson noise thermometry. The graphene device, together with a bias-T, is placed in an oxygen-free copper block on the 0.3 K cold stage of a sorption cooler. The integration of the bias-T allows a function generator to apply a modulated square wave voltage excitation at 2 kHz with a duty cycle of 50% and a modulation depth of 100% to heat the graphene microbridge. This setup enables measurement of the noise power responsivity of the graphene device via a lock-in amplifier. In our case, the voltage excitation amplitude is only several tens of microvolts, exerting negligible influence on the bias-T's operation near the graphene device. The Johnson noise signal from the device is transmitted through a superconducting NbTi coaxial cable to a cryogenic low-noise amplifier fixed on the 4 K cold stage of the cooler. After passing through the cryogenic low-noise amplifier with a gain of 36 ± 3 dB, the Johnson noise signal is further amplified by a 30 dB room-temperature amplifier (operating at 300 K). Subsequently, the signal undergoes filtration through a bandpass filter (spanning from 0.5 to 1.8 GHz) to define the readout bandwidth and then passes through a square-law detector (with a sensitivity of ∼1 mV/μW) for readout. Finally, a lock-in amplifier is utilized to measure the signal

https://doi.org/10.1021/acsomega.4c02727
ACS Omega 2024, 9, 23053−23059

response, while a fast Fourier transform (FFT) analyzer is employed to determine the spectral density of the signal power. Here, the Johnson noise power can be written as

$$P_J = k_B(T_e + T_{\text{Readout}})\eta G_{amp} B \quad (1)$$

where k_B is the Boltzmann constant, T_e is the electron temperature, $T_{Readout}$ is the noise temperature of the readout system, η is the coupling between the graphene device and the cryogenic low-noise amplifier, and G_{amp} and B are the gain and the bandwidth of the entire Johnson noise readout system, respectively. In our case, the noise temperature of the readout system $T_{Readout}$ is estimated to be around 5.4 K from the measured the temperature-dependent noise power of the graphene device.[14] Additionally, the coupling between the graphene device and the cryogenic low-noise amplifier is found to be greater than 0.85, as indicated by $\eta = (4R_0R_L)/(R_0 + R_L)^2$, with R_0 and R_L (about 50 Ω) being the resistances of the graphene device and the cryogenic low-noise amplifier, respectively. Therefore, our readout system does not require any impedance matching circuit, such as an inductor-capacitor matching network.[2,13]

RESULTS AND DISCUSSION

Figure 2(a) shows the measured thermal conductance of three graphene devices with the microbridge lengths of 2.7, 4.6, and 8.8 μm at bath temperatures ranging from 0.3 to 15 K. Here a heating resistor is installed on the 0.3 K cold stage of the sorption cooler to adjust the bath temperature. After raising the temperature of the 0.3 K cold stage to 15 K, it is necessary to recycle the 0.3 K sorption cooler to return it to its initial temperature of 0.3 K. It should be noted that temperatures exceeding 15 K could influence the temperature of the 4 K cold stage of the sorption cooler, potentially impacting the gain of the cryogenic low-noise amplifier. The thermal conductance (defined as $G = \Delta P_{in}/\Delta T_e$) of the graphene device is obtained by applying a small modulated dc Joule heating power ($\Delta P_{in} = I^2R$) to the device and then measuring its noise power responsivity as well as electron temperature responsivity. As depicted in Figure 2(a), a crossover from cubic to linear temperature dependence is observed at a specific temperature in the measured thermal conductance. Notably, the crossover temperature is found to be associated with the length of the microbridge, and the longer the microbridge is, the lower the crossover temperature is. In our case, the crossover temperatures for graphene devices with microbridge lengths of 8.8 and 4.6 μm are 7 and 10.4 K, respectively. However, when the graphene microbridge is reduced to 2.7 μm, the crossover temperature exceeds the measurable temperature range (up to 15 K), reaching approximately 20.8 K according to the calculated result. In Figure 2(a), all of these crossover temperatures are labeled to emphasize the different temperature dependences for thermal conductance. We attribute this crossover phenomenon to the switching from electron−phonon coupling to electron diffusion in the graphene microbridge. Below the crossover temperature, the thermal transport in the graphene device is governed by electron diffusion and the thermal conductance exhibits an almost proportional relationship to temperature. Above the crossover temperature, the thermal conductance resulting from electron−phonon coupling follows the established theory, displaying a temperature power of T^3 at $T_x < T_e < T_{BG}$ (the temperature range within which our graphene device operates). Here, T_x is a transition temperature defined as[23]

$$T_x = 30\hbar s\zeta(3)/(\pi^4 k_B l_e) \quad (2)$$

where $s = 2 \times 10^4$ m/s is the speed of sound in graphene.[23] Our estimation indicates that the transition temperature T_x is approximately 0.34 K. At temperatures below T_x, it is predicted that the electron−phonon coupling is enhanced due to the disorder-assisted scattering.[23] In addition, T_{BG} denotes the Bloch−Gruneisen temperature and is defined as[24]

$$T_{BG} = 2(s/v)(\phi_1 E_F)^{0.5}/k_B \quad (3)$$

where $\phi_1 = 390$ meV is the interlayer coupling amplitude,[25] $v = 10^6$ m/s is the Fermi velocity, and $E_F = 395$ meV (derived from $\hbar^2\pi n/2m$, where the effective mass of bilayer graphene $m = 0.037m_e$, and $m_e = 9.1 \times 10^{-31}$ kg represents the electron mass) is the Fermi energy.[22,23] In our case, the Bloch−Gruneisen temperature T_{BG} is estimated to be about 182 K. Figure 2(a) also shows the simulated results based on a distributed hot spot model.[18,21] Here, we assume that the phonon temperature in graphene is equal to the bath temperature because the phonon-substrate coupling constant is typically much larger than the electron−phonon coupling constant in graphene.[4,36] The model relies on solving a heat balance equation for position-dependent electron temperature $T_e(x)$ in the graphene microbridge

$$I^2R = -LW\frac{\partial}{\partial x}\left(k_{WF}(x)\frac{\partial T_e(x)}{\partial x}\right) + LW\sigma_{ep}(T_e^N(x) - T_0^N) \quad (4)$$

where I^2R is the dc Joule heating on the microbridge, L and W are the microbridge length and width, respectively. σ_{ep} is the electron−phonon coupling efficiency, N is an exponent related to the electron−phonon coupling in graphene, and T_0 is the phonon temperature. Additionally, $k_{WF}(x) = L_0T_e(x)L/(WR)$ is the electron thermal conductivity, where L_0 is the Lorenz number and equals 2.45×10^{-8} W Ω K^{-2}. It can be seen that the simulated results in Figure 2(a) are in good agreement with the measured results. In the presence of impurity scattering in graphene, a modification of the Lorenz number is usually expected.[13,18] However, we did not make any corrections to the Lorenz number L_0 in the simulation. It suggests that the graphene obtained through hydrogen intercalation possesses properties closer to pristine graphene.[26] Furthermore, the electron−phonon coupling efficiency σ_{ep} is determined be about 0.18 W K^{-4} m^{-2}, significantly smaller than the phonon-substrate coupling efficiency σ_K, approximately 2×10^3 W K^{-4} m^{-2}. The phonon-substrate coupling efficiency is calculated based on the graphene/SiC thermal contact resistance, which is about 0.5×10^{-9} m^2 K W^{-1} at 100 K, and then roughly estimated via T^3 extrapolation.[37] Subsequently, the deformation potential D of the graphene device can be estimated in terms of $\sigma_{ep} = (\pi^2D^2\phi_1k_B^4/60\rho\hbar^5v^3s^3)(\phi_1E_F)^{0.5}$,[24] resulting in a value of 55 eV, which is consistent with the range of values obtained by other experiments.[13,27]

Figure 2 (b) displays the calculated temperature distributions of three graphene devices with microbridge lengths of 2.7, 4.6, and 8.8 μm, at bath temperatures of 0.3, 7, and 15 K, respectively. It is evident that at 15 K, as the microbridge length increases from 2.7 to 8.8 μm, the temperature distribution gradually flattens, particularly in the middle of the microbridge, where the bottleneck in cooling is attributed

https://doi.org/10.1021/acsomega.4c02727
ACS Omega 2024, 9, 23053−23059

to the electron−phonon coupling. At 0.3 K, electron diffusion dominates in all three graphene devices, resulting in nearly identical temperature distributions across the microbridges, with a pronounced temperature gradient. In the absence of electron diffusion in the microbridge, the electron temperature becomes position-independent and is given by $T_e(x) = (I^2R/LW\sigma_{ep} - T_0^n)^{1/n}$.[18] Figure 3 shows the calculated thermal

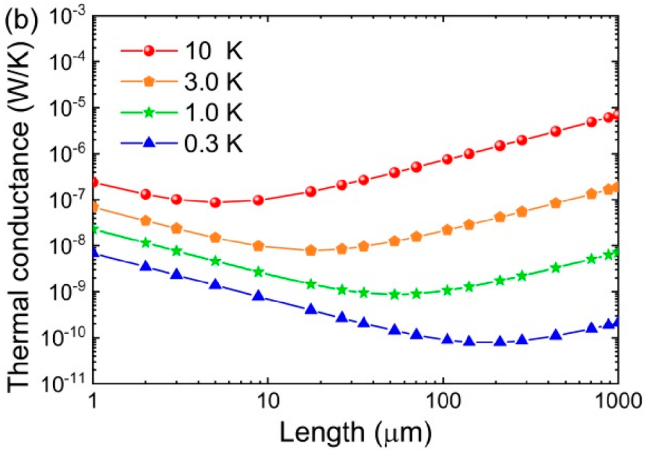

Figure 3. Calculated thermal conductance for the graphene device as a function of the microbridge length at different bath temperatures.

conductance for different microbridge lengths (varying from 1 to 1000 μm) at different bath temperatures. It is obvious that with an increase in microbridge length the thermal conductance of the graphene device initially decreases and then increases. Here, the microbridge length associated with the minimum thermal conductance corresponds to similar contributions from electron diffusion and electron−phonon interaction, indicating the equality of the electron diffusion length L_{dif} and the electron−phonon interaction length $L_{e\text{-}ph}$ in the graphene microbridge. Given that the electron diffusion length L_{dif} is approximately equal to L/π,[28] we conclude that the microbridge length corresponding to the minimum thermal conductance can be given by $\pi L_{e\text{-}ph}$. When the microbridge length is less than $\pi L_{e\text{-}ph}$, the thermal transport in the graphene device is primarily governed by the electron diffusion, and the thermal conductance due to the electron diffusion is inversely proportional to the length (i.e., the resistance) of the microbridge, as expressed by $12L_0T_e/R$. Conversely, when the microbridge length is greater than $\pi L_{e\text{-}ph}$, the thermal transport in the graphene device is mainly determined by the electron−phonon coupling, and the thermal conductance due to the electron−phonon coupling is almost proportional to the length of the microbridge, as indicated by $NLW\sigma_{ep}T_e^{N-1}$.[18] In addition, the electron−phonon interaction length $L_{e\text{-}ph}$ is closely dependent upon temperature. As the temperature increases from 0.3 to 10 K, the electron−phonon interaction length $L_{e\text{-}ph}$ decreases from $200/\pi$ μm to $5/\pi$ μm. Additionally, we assessed the value of the electron−phonon interaction length $L_{e\text{-}ph}$ at 0.3 K using the formula $L_{e\text{-}ph} = (D_e\tau_{eph})^{0.5} = (D_eC_e/G_{e\text{-}ph})^{0.5} = (D_e\pi^2DOSk_B^2T/(3G_{e\text{-}ph}))^{0.5} = (\pi^2k_B^2T/(3e^2RN\sigma_{ep}T^{N-1}))^{0.5} = 58$ μm, which closely aligns with the result obtained from hot spot modeling ($\sim 200/\pi$ μm). Here, $DOS = 1/(e^2RD_e)$ represents the two-dimensional density of states, where D_e is the electron diffusion coefficient, and $\tau_{e\text{-}ph}$ is the electron−phonon interaction time. Additionally, by utilizing the above relationship and $\tau_{e\text{-}ph} = A\gamma T/G_{e\text{-}ph}$, where A represents the area of the graphene microbridge and $\gamma = 2\pi E_F k_B^2/(3\hbar^2v^2)$ serves as the Sommerfeld coefficient, we can extract D_e in graphene.[24] In our case, electron diffusion coefficient D_e is estimated to be around 993 cm^2/s. Furthermore, we utilized the Einstein relation $D_e = \mu E_F/e$ to calculate the theoretical electron diffusion coefficient,[29] yielding a value of about 1600 cm^2/s. Here, the estimated value closely approximates the theoretical value. This finding is also comparable to the results reported in other studies.[30−32] Note that the electron diffusion coefficient D_e is closely related to the substrate material owing to the impact of surface polar phonons.[30] Furthermore, impurity scattering in graphene may also play a role in the modulation of the electron diffusion coefficient D_e.[31]

It is of particular interest to study the impact of an external magnetic field on the thermal transport of a graphene device. Figure 4 illustrates the measured thermal conductance of the

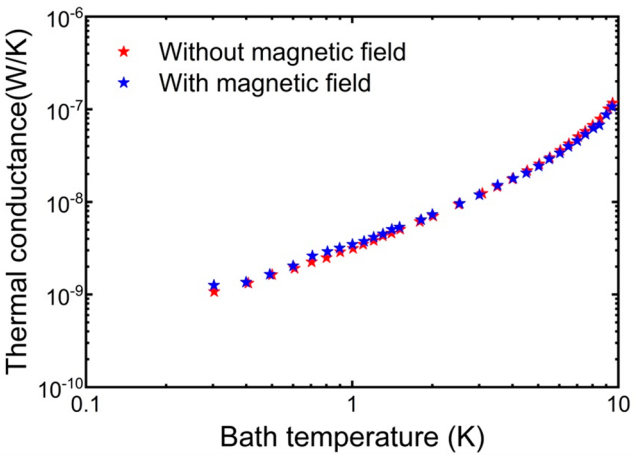

Figure 4. Measured thermal conductance of the graphene device with a microbridge length of 8.8 μm at different temperatures with and without an external magnetic field.

graphene device with a microbridge length of 8.8 μm at different temperatures with and without the presence of a magnetic field. Here, the magnetic field is generated by a permanent magnet attached to the copper block used to mount the graphene device. The magnetic field produced by the permanent magnet is measured using a linear Hall effect sensor in a separate experiment[33] and is found to be about 0.38 T. As depicted in Figure 4, the difference in thermal conductance is minimal before and after applying the magnetic field. It has been understood that the thermal conductance of the graphene device is primarily determined by the electron diffusion at low temperatures. Previous study shows that within the temperature range of $0.01 < k_BT/E_F < 0.7$, the thermal conductance due to electron diffusion in graphene exhibits a dependence on the magnetic field due to charged impurities.[34] However, the operating temperature of our graphene devices falls outside this range. Specifically, at 15 K, which is the maximum bath temperature our measurement setup can achieve, the value of k_BT/E_F for our graphene devices is approximately equal to 0.003. In other words, significant differences in thermal conductance before and after the application of the magnetic field should be observable only when the bath temperature reaches around 50 K. Unfortunately, our measurement setup cannot achieve such high bath temperature. Consequently, the thermal conductance of the graphene device exhibits a weak

https://doi.org/10.1021/acsomega.4c02727
ACS Omega 2024, 9, 23053−23059

dependence on the magnetic field. This feature is actually beneficial for the development of graphene-based detectors as it provides the detector with excellent anti-interference capabilities.

We also characterized the noise equivalent power (NEP) of three graphene devices using Johnson noise thermometry.[15] Figure 5 shows the measured electrical NEP of the graphene

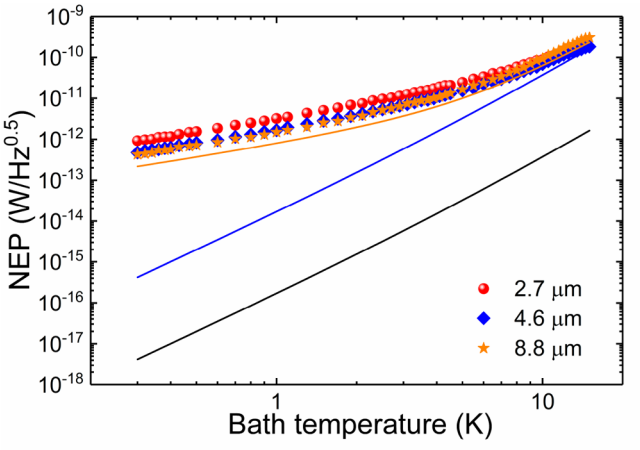

Figure 5. Measured and calculated electrical NEP values of three graphene devices. The measured NEP of three graphene devices is indicated by different symbols. The calculated results are specific to the graphene device with a microbridge length of 8.8 μm, encompassing scenarios involving electron diffusion (orange line), excluding electron diffusion (blue line), and for the graphene device with a reduced microbridge size (black line).

devices at different bath temperatures. It can be seen that the measured NEP decreases as the microbridge length increases and the measured NEP of the graphene device with a microbridge length of 8.8 μm is about 0.43 pW/Hz$^{0.5}$ at 0.3 K. The NEP of a detector employing Johnson noise thermometry is mainly determined by the thermal conductance and can be expressed as

$$NEP = (T_e + T_{\text{Readout}})G/(0.5B)^{0.5} \quad (5)$$

where G is the thermal conductance of the detector. Using this formula, we calculated the NEP of the graphene device with a microbridge length of 8.8 μm at different bath temperatures, and the results agree well with the measured data, as depicted in Figure 5, which also includes the calculated thermal conductance of the graphene device as a function of the bath temperature. It is recognized that at low temperatures, the thermal conductance G is primarily governed by the electron diffusion in graphene. Consequently, enhancing the sensitivity of the graphene device can be achieved by mitigating the electron diffusion, for example, through the use of superconductors as electrodes.[15] After the electron diffusion was eliminated, the NEP of the graphene device can be as low as 10^{-15} W/Hz$^{0.5}$ at 0.3 K, as shown in Figure 5. Furthermore, the sensitivity of the graphene device can be further improved by reducing the dimensions of the graphene microbridge to decrease the thermal conductance resulting from the electron–phonon coupling. If both the length and width of the microbridge are reduced by a factor of 10, then the NEP of the graphene device could potentially reach 10^{-17} W/Hz$^{0.5}$ at 0.3 K (see Figure 5), making it comparable to other superconducting detectors, such as the superconducting transition edge sensor (TES) detector.[35] It is worth noting that with a significantly reduced thermal conductance, the thermal radiation from the cryogenic low-noise amplifier at microwave frequencies may potentially impact the operation of the graphene device.[15] Additionally, when the graphene microbridge becomes sufficiently short, the Josephson coupling induced by proximity effect may occur, potentially affecting the operation of the graphene device with Johnson noise thermometry,[12] which merits further study in the future.

CONCLUSIONS

We thoroughly studied the thermal transport of graphene microbridges with varying microbridge lengths at different bath temperatures. We find that with the increase in the bath temperature, the thermal transport in the microbridges switches from electron diffusion to electron–phonon coupling, and the switching temperature is closely related to the microbridge length. Based on the length-dependent switching temperature, we have determined the electron diffusion coefficient D_e of the graphene microbridge to be about 993 cm^2/s. Furthermore, the deformation potential D of the graphene microbridge was estimated to be around 55 eV. Additionally, we find that the thermal conductance of the graphene microbridge is nearly independent of the magnetic field. This characteristic proves advantageous for the development of graphene-based detectors, endowing them with excellent anti-interference capabilities.

AUTHOR INFORMATION

Corresponding Authors

Zhihong Feng − *National Key Laboratory of Solid-State Microwave Devices and Circuits, Shijiazhuang 050051, China*; Email: ga917vv@163.com

Wei Miao − *Purple Mountain Observatory, Chinese Academy of Sciences, Nanjing 210033, China*; Email: weimiao@pmo.ac.cn

Authors

Feiming Li − *Purple Mountain Observatory, Chinese Academy of Sciences, Nanjing 210033, China; University of Science and Technology of China, Hefei 230026, China*; orcid.org/0009-0009-8627-0127

Cui Yu − *National Key Laboratory of Solid-State Microwave Devices and Circuits, Shijiazhuang 050051, China*; orcid.org/0000-0002-6346-5943

Zezhao He − *National Key Laboratory of Solid-State Microwave Devices and Circuits, Shijiazhuang 050051, China*

Qingcheng Wang − *Purple Mountain Observatory, Chinese Academy of Sciences, Nanjing 210033, China; University of Science and Technology of China, Hefei 230026, China*

Jiaqiang Zhong − *Purple Mountain Observatory, Chinese Academy of Sciences, Nanjing 210033, China*

Feng Wu − *Purple Mountain Observatory, Chinese Academy of Sciences, Nanjing 210033, China*

Zheng Wang − *Purple Mountain Observatory, Chinese Academy of Sciences, Nanjing 210033, China*

Kangmin Zhou − *Purple Mountain Observatory, Chinese Academy of Sciences, Nanjing 210033, China*

Yuan Ren − *Purple Mountain Observatory, Chinese Academy of Sciences, Nanjing 210033, China*; orcid.org/0000-0002-7903-7556

https://doi.org/10.1021/acsomega.4c02727
ACS Omega 2024, 9, 23053−23059

Wen Zhang − *Purple Mountain Observatory, Chinese Academy of Sciences, Nanjing 210033, China*
Jing Li − *Purple Mountain Observatory, Chinese Academy of Sciences, Nanjing 210033, China*
Shengcai Shi − *Purple Mountain Observatory, Chinese Academy of Sciences, Nanjing 210033, China*
Qingbin Liu − *National Key Laboratory of Solid-State Microwave Devices and Circuits, Shijiazhuang 050051, China*

Complete contact information is available at: https://pubs.acs.org/10.1021/acsomega.4c02727

Author Contributions

F.L.: Investigation, Formal analysis, Writing−original draft; W.M.: Conceptualization, Supervision, Writing−review and editing; C.Y.: Resources; Z.H.: Investigation, Resources; Q.W.: Investigation; J.Z.: Methodology, Formal analysis; F.W.: Investigation; Z.W.: Investigation, Resources; K.Z.: Investigation, Validation; Y.R.: Investigation; W.Z.: Investigation; J.L.: Investigation; S.S.: Conceptualization, Supervision, Writing−review and editing; Q.L.: Resources; Z.F.: Resources.

Notes

The authors declare no competing financial interest.

■ ACKNOWLEDGMENTS

This work was supported in part by the National Key R&D Program of China under Grant No. 2021YFC2203404 and in part by the National Natural Science Foundation of China (NSFC) under Grant Nos. 12321003 and 12020101002.

■ REFERENCES

(1) Fong, K. C.; Schwab, K. C. Ultrasensitive and Wide-Bandwidth Thermal Measurements of Graphene at Low Temperatures. *Phys. Rev. X* **2012**, *2* (3), No. 031006.
(2) Crossno, J.; Shi, J. K.; Wang, K.; Liu, X.; Harzheim, A.; Lucas, A.; Sachdev, S.; Kim, P.; Taniguchi, T.; Watanabe, K.; Ohki, T. A.; Fong, K. C. Observation of the Dirac Fluid and the Breakdown of the Wiedemann-Franz Law in Graphene. *Science* **2016**, *351* (6277), 1058−1061.
(3) Hwang, E. H.; Das Sarma, S. Acoustic Phonon Scattering Limited Carrier Mobility in Two-Dimensional Extrinsic Graphene. *Phys. Rev. B* **2008**, *77* (11), No. 115449.
(4) Yan, J.; Kim, M.-H.; Elle, J. A.; Sushkov, A. B.; Jenkins, G. S.; Milchberg, H. M.; Fuhrer, M. S.; Drew, H. D. Dual-Gated Bilayer Graphene Hot-Electron Bolometer. *Nat. Nanotechnol.* **2012**, *7* (7), 472−478.
(5) El Fatimy, A.; Myers-Ward, R. L.; Boyd, A. K.; Daniels, K. M.; Gaskill, D. K.; Barbara, P. Epitaxial Graphene Quantum Dots for High-Performance Terahertz Bolometers. *Nat. Nanotechnol.* **2016**, *11* (4), 335−338.
(6) Han, Q.; Gao, T.; Zhang, R.; Chen, Y.; Chen, J.; Liu, G.; Zhang, Y.; Liu, Z.; Wu, X.; Yu, D. Highly Sensitive Hot Electron Bolometer Based on Disordered Graphene. *Sci. Rep.* **2013**, *3* (1), 3533.
(7) Qin, H.; Sun, J.; Liang, S.; Li, X.; Yang, X.; He, Z.; Yu, C.; Feng, Z. Room-Temperature, Low-Impedance and High-Sensitivity Terahertz Direct Detector Based on Bilayer Graphene Field-Effect Transistor. *Carbon* **2017**, *116*, 760−765.
(8) Gayduchenko, I.; Xu, S. G.; Alymov, G.; Moskotin, M.; Tretyakov, I.; Taniguchi, T.; Watanabe, K.; Goltsman, G.; Geim, A. K.; Fedorov, G.; Svintsov, D.; Bandurin, D. A. Tunnel Field-Effect Transistors for Sensitive Terahertz Detection. *Nat. Commun.* **2021**, *12* (1), 543.
(9) Vicarelli, L.; Vitiello, M. S.; Coquillat, D.; Lombardo, A.; Ferrari, A. C.; Knap, W.; Polini, M.; Pellegrini, V.; Tredicucci, A. Graphene Field-Effect Transistors as Room-Temperature Terahertz Detectors. *Nat. Mater.* **2012**, *11* (10), 865−871.
(10) Lee, G.-H.; Efetov, D. K.; Jung, W.; Ranzani, L.; Walsh, E. D.; Ohki, T. A.; Taniguchi, T.; Watanabe, K.; Kim, P.; Englund, D.; Fong, K. C. Graphene-Based Josephson Junction Microwave Bolometer. *Nature* **2020**, *586* (7827), 42−46.
(11) Kokkoniemi, R.; Girard, J.-P.; Hazra, D.; Laitinen, A.; Govenius, J.; Lake, R. E.; Sallinen, I.; Vesterinen, V.; Partanen, M.; Tan, J. Y.; et al. Bolometer Operating at the Threshold for Circuit Quantum Electrodynamics. *Nature* **2020**, *586* (7827), 47−51.
(12) Miao, W.; Li, F.; Luo, Q.; Wang, Q.; Zhong, J.; Wang, Z.; Zhou, K.; Ren, Y.; Zhang, W.; Li, J.; Shi, S.; Yu, C.; He, Z.; Liu, Q.; Feng, Z. A Terahertz Detector Based on Superconductor-Graphene-Superconductor Josephson Junction. *Carbon* **2023**, *202*, 112−117.
(13) Fong, K. C.; Wollman, E. E.; Ravi, H.; Chen, W.; Clerk, A. A.; Shaw, M. D.; Leduc, H. G.; Schwab, K. C. Measurement of the Electronic Thermal Conductance Channels and Heat Capacity of Graphene at Low Temperature. *Phys. Rev. X* **2013**, *3* (4), No. 041008.
(14) Miao, W.; Gao, H.; Wang, Z.; Zhang, W.; Ren, Y.; Zhou, K. M.; Shi, S. C.; Yu, C.; He, Z. Z.; Liu, Q. B.; Feng, Z. H. A Graphene-Based Terahertz Hot Electron Bolometer with Johnson Noise Readout. *J. Low Temp. Phys.* **2018**, *193* (3−4), 387−392.
(15) Miao, W.; Li, F. M.; He, Z. Z.; Gao, H.; Wang, Z.; Zhang, W.; Ren, Y.; Zhou, K. M.; Zhong, J. Q.; Shi, S. C.; et al. Demonstration of a High-Sensitivity and Wide-Dynamic-Range Terahertz Graphene Hot-Electron Bolometer with Johnson Noise Thermometry. *Appl. Phys. Lett.* **2021**, *118* (1), No. 013104.
(16) Borzenets, I. V.; Coskun, U. C.; Mebrahtu, H. T.; Bomze, Yu. V.; Smirnov, A. I.; Finkelstein, G. Phonon Bottleneck in Graphene-Based Josephson Junctions at Millikelvin Temperatures. *Phys. Rev. Lett.* **2013**, *111* (2), No. 027001.
(17) Baker, A. M. R.; Alexander-Webber, J. A.; Altebaeumer, T.; Nicholas, R. J. Energy Relaxation for Hot Dirac Fermions in Graphene and Breakdown of the Quantum Hall Effect. *Phys. Rev. B* **2012**, *85* (11), No. 115403.
(18) Zihlmann, S.; Makk, P.; Castilla, S.; Gramich, J.; Thodkar, K.; Caneva, S.; Wang, R.; Hofmann, S.; Schönenberger, C. Non-equilibrium Properties of Graphene Probed by Superconducting Tunnel Spectroscopy. *Phys. Rev. B* **2019**, *99* (7), No. 075419.
(19) Yu, C.; Liu, Q.; Li, J.; Lu, W.; He, Z.; Cai, S.; Feng, Z. Preparation and Electrical Transport Properties of Quasi Free Standing Bilayer Graphene on SiC (0001) Substrate by H Intercalation. *Appl. Phys. Lett.* **2014**, *105* (18), No. 183105.
(20) He, Z.; Yu, C.; Liu, Q.; Song, X.; Gao, X.; Guo, J.; Zhou, C.; Cai, S.; Feng, Z. High Temperature RF Performances of Epitaxial Bilayer Graphene Field-Effect Transistors on SiC Substrate. *Carbon* **2020**, *164*, 435−441.
(21) Miao, W.; Zhang, W.; Zhong, J. Q.; Shi, S. C.; Delorme, Y.; Lefevre, R.; Feret, A.; Vacelet, T. Non-Uniform Absorption of Terahertz Radiation on Superconducting Hot Electron Bolometer Microbridges. *Appl. Phys. Lett.* **2014**, *104* (5), No. 052605.
(22) Zhu, W.; Perebeinos, V.; Freitag, M.; Avouris, P. Carrier Scattering, Mobilities, and Electrostatic Potential in Monolayer, Bilayer, and Trilayer Graphene. *Phys. Rev. B* **2009**, *80* (23), No. 235402.
(23) Chen, W.; Clerk, A. A. Electron-Phonon Mediated Heat Flow in Disordered Graphene. *Phys. Rev. B* **2012**, *86* (12), No. 125443.
(24) Viljas, J. K.; Heikkilä, T. T. Electron-Phonon Heat Transfer in Monolayer and Bilayer Graphene. *Phys. Rev. B* **2010**, *81* (24), No. 245404.
(25) Koshino, M.; Ando, T. Orbital Diamagnetism in Multilayer Graphenes: Systematic Study with the Effective Mass Approximation. *Phys. Rev. B* **2007**, *76* (8), No. 085425.
(26) Johannsen, J. C.; Ulstrup, S.; Bianchi, M.; Hatch, R.; Guan, D.; Mazzola, F.; Hornekær, L.; Fromm, F.; Raidel, C.; Seyller, T.; Hofmann, P. Electron−Phonon Coupling in Quasi-Free-Standing Graphene. *J. Phys.: Condens. Matter* **2013**, *25* (9), No. 094001.

(27) Efetov, D. K.; Kim, P. Controlling Electron-Phonon Interactions in Graphene at Ultrahigh Carrier Densities. *Phys. Rev. Lett.* **2010**, *105* (25), No. 256805.
(28) Miao, W. Investigation of Hot Electron Bolometer Mixers for Submillimeter Multi-pixel Receiver Applications. Ph.D. thesis, LERMA laboratory, Observatoire de Paris, Paris, France, 2010.
(29) Rengel, R.; Martín, M. J. Diffusion Coefficient, Correlation Function, and Power Spectral Density of Velocity Fluctuations in Monolayer Graphene. *J. Appl. Phys.* **2013**, *114* (14), No. 143702.
(30) Rengel, R.; Pascual, E.; Martín, M. J. Influence of the Substrate on the Diffusion Coefficient and the Momentum Relaxation in Graphene: The Role of Surface Polar Phonons. *Appl. Phys. Lett.* **2014**, *104* (23), No. 233107.
(31) Chen, K.; Yogeesh, M. N.; Huang, Y.; Zhang, S.; He, F.; Meng, X.; Fang, S.; Sheehan, N.; Tao, T. H.; Bank, S. R.; Lin, J.-F.; Akinwande, D.; Sutter, P.; Lai, T.; Wang, Y. Non-Destructive Measurement of Photoexcited Carrier Transport in Graphene with Ultrafast Grating Imaging Technique. *Carbon* **2016**, *107*, 233−239.
(32) Ruzicka, B. A.; Wang, S.; Werake, L. K.; Weintrub, B.; Loh, K. P.; Zhao, H. Hot Carrier Diffusion in Graphene. *Phys. Rev. B* **2010**, *82* (19), No. 195414.
(33) Miao, W.; Li, F.; Gao, H.; Zhou, K.; Zhong, J.; Ren, Y.; Zhang, W.; Shi, S.; Delorme, Y. Linear and Nonlinear Flux-Flow Behaviors in Superconducting Hot-Electron Bolometer Mixers. *Appl. Phys. Lett.* **2021**, *118* (11), No. 112602.
(34) Crisan, M.; Grosu, I.; Tifrea, I. Magnetic Field Effects on the Thermoelectric Properties of Monolayer Graphene. *Phys. E: Low-dimens. Syst. and Nanostruct.* **2020**, *124*, No. 114361.
(35) Luo, Q.; Zhong, J.; Miao, W.; Li, F.; Wang, Q.; Ding, J.; Wu, F.; Wang, Z.; Zhou, K.; Ren, Y.; Zhang, W.; Li, J.; Shi, S. A 220 GHz superconducting titanium transition edge sensor array developed for cosmic microwave background experiments. *Supercond. Sci. Technol.* **2023**, *36*, No. 115004.
(36) Betz, A. C.; Jhang, S. H.; Pallecchi, E.; Ferreira, R.; Fève, G.; Berroir, J.-M.; Plaçais, B. Supercollision Cooling in Undoped Graphene. *Nat. Phys.* **2013**, *9* (2), 109−112.
(37) Wang, Z.; Bi, K.; Guan, H.; Wang, J. Thermal Transport between Graphene Sheets and SiC Substrate by Molecular-Dynamical Calculation. *J. Mater.* **2014**, *2014*, 479808.

https://doi.org/10.1021/acsomega.4c02727
ACS Omega 2024, 9, 23053−23059